Modular Imaging Scaffold for Single-Particle Electron Microscopy

Nesrine Aissaoui, Josephine Lai Kee Him, Allan Mills, Nathalie Declerck, Zakia Morichaud, Konstantin Brodolin, Sonia Baconnais, Eric Le Cam, Jean-Baptiste Charbonnier, Rémy Sounier, et al.

Modular imaging scaffold for single-particle electron microscopy

Nesrine Aissaoui[a, b#], Josephine Lai-Kee-Him[a, b#], Allan Mills[a, b], Nathalie Declerck[a, b, c], Zakia Morichaud[b, e], Konstantin Brodolin[b, e], Sonia Baconnais[g], Eric Le Cam[g], Jean Baptiste Charbonnier[f], Rémy Sounier[b, d], Sébastien Granier[b, d], Virginie Ropars[f], Patrick Bron[a, b*], Gaetan Bellot[a, b*]*

[a] Centre de Biochimie Structurale, CNRS UMR 5048, INSERM U1054, F-34000 Montpellier, France.

[b] Université de Montpellier, F-34000 Montpellier, France.

[c] INRA, Departement MICA, 78352 Jouy-en-Josas, France.

[d] Institut de Génomique Fonctionnelle, CNRS UMR 5203, INSERM U1191, F-34000 Montpellier, France.

[e] IRIM, CNRS, Université Montpellier, 1919 route de Mende, 34293, Montpellier, France.

[f] Université Paris-Saclay, CEA, CNRS, Institute for Integrative Biology of the Cell (I2BC), 91198, Gif-sur-Yvette, France.

[g] Signalisations, Noyaux et Innovations en Cancérologie, UMR 8126, CNRS, Université Paris-Sud, Gustave Roussy, Université Paris-Saclay, Villejuif, France.

* To whom correspondence should be addressed, electronic mail: gaetan.bellot@cbs.cnrs.fr; patrick.bron@cbs.cnrs.fr; virginie.ropars@i2bc.paris-saclay.fr

ABSTRACT: Technological breakthroughs in electron microscopy (EM), open new opportunities and raise novel challenges, specifically related to sample preparation and heterogeneous macromolecular assemblies such as, DNA-protein, protein-protein and membrane protein assemblies. Here, we built a V-shaped DNA origami as a scaffolding molecular system to template proteins at user-defined positions in space. This template positions macromolecular assemblies of various sizes up to 47 nm in diameter, juxtaposes combinations of biomolecules into complex arrangements, isolates biomolecules in their active state, and stabilizes membrane proteins in solution. In addition, the design can be engineered to tune DNA mechanical properties by exerting a controlled piconewton (pN) force on the molecular system and thus adapted to characterize mechano-sensitive proteins. The binding site can also be specifically customized to accommodate the protein of interest, either interacting spontaneously with DNA or through directed chemical conjugation, increasing the range of potential targets for single-particle EM investigation. We assessed the applicability for five different proteins. Finally, as a proof of principle, we used RNAP protein to validate the approach and to explore the compatibility of the template with cryo-EM sample preparation.

KEYWORDS: DNA origami, Nanotechnology, molecular template, electron microscopy, single particles imaging.

DNA nanotechnology enables the bottom-up self-assembly of arbitrarily shaped, rigid, three-dimensional (3D) nano-objects with precise subnanometer features and with molecular weights up to the gigadalton scale.[1–3] Self-assembled DNA origami are made from a scaffold strand of single-stranded DNA (ssDNA), typically M13 phage genomic DNA, which is folded by, on average, 200 short staple strands,[1, 4] which can be specifically functionalized and modified with chemical groups and biomolecules.[5, 6] The DNA origami method is one of the most efficient ways to enable accurate molecular scale positioning or to juxtapose combinations of these elements into complex arrange-ments.[7] This is why bottom-up DNA self-assembly has become a particularly promising area for nanofabrication to create tunable plasmonic,[8] drug delivery systems,[9] or as a molecular template for different applications,[10, 11] including the incorporation of proteins for EM analysis.[12, 13]

Beyond recent technological improvements,[14, 15] EM techniques open new opportunities and raise novel challenges, specifically related to sample preparation and heterogeneous macromolecular assemblies (i.e., DNA-protein, protein-protein and membrane proteins assemblies). In sample preparation, the primary limiting factor for single-particle visualization is the grid preparation. In practice, an ideal EM-grid for both negative stain or frozen hydrated sample collection would have the majority of areas maximally occupied, with well-dispersed, and randomly oriented particles.[16] Numerous methodologies have been developed to optimize cryo-EM grid preparations,[17, 18] such as buffer composition, the type and concentration of

surfactants,[19, 20] protein concentrations,[21] or the plunge-freezing duration.[22] In addition, increasing the stability of macromolecular assemblies is crucial for their successful EM investigation. However, most rational stabilization strategies relied on thermostabilization or chemical cross-linking methods, with the potential to induce artefacts caused by mutations or chemical fixation.

Two previous studies proposed to use self-assembled DNA nanostructures as an alternative approach to obtain optimal grids for data collection.[12, 13] In the first study, Daniele N. Selmi and co-authors proposed the use of a self-assembled 2D-DNA nanotemplate to create non-overlapping arrays of membrane proteins.[12] However, in their design, the protein arranged on a hexagonal lattice is difficult to visualize and isolate, which hindered the extraction and analysis of single-particles. In the second study, Thomas G. Martin and co-authors, developed a hollow pillar DNA origami structure dedicated to 3D tomography reconstruction of DNA binding protein by enclosing the p53 tetramer inside a central cavity of 13.2 × 13.6 nm.[13] Several limitations were reported in their DNA support structure's design. This includes, (i) the small cavity size limiting the accessibility of the protein to the binding site which led to low particle yield, i.e., 77% of the remaining support structures did not bind their target protein, (ii) five different designs of DNA origami have to be created and analyzed by cryo-EM to record five different orientations to cover the entire 180° of a tomographic tilt series which is technically possible if the protein binds to a perfectly rigid DNA nanostructure, (iii) the structure is not rigid enough to exert control over the orientations of proteins to calculate a tomographic 3D re-construction, in addition, 42% of the support structures did not incorporate the tilt axis, (iv) the nanotemplate is designed for cryo-EM only, and specifically for tomography. Characterization

and visualization by negative stain of any biomolecule encapsulated on this DNA origami-support is impossible.

Here, we propose a new design of DNA origami that overcomes the main limitations of the previously proposed designs and proves adapted to multi-protein complexes. We designed a V-shaped structure that contains a double-strand (ds) DNA helix "segment" in-between its two "arms" (**Figure 1a**). This dsDNA helix has been designed with a single-strand (ss) break at each side to provide the freedom rotation of the connected dsDNA-binding domain. The binding site is engineered with a customizable DNA sequence or chemical modification to specifically bind a target biomolecule. To image a maximum of biomolecule orientations from a designed single molecular system, an assembly strategy is conceived to combine two monomer origami together to act as a single platform able to hold two separate target biomolecules (**Figure 1b**). The physical properties of the V-shaped DNA-design presents several advantages it : (i) facilitates the localization of large target biomolecules (up to 47 nm diameter size), specifically enclosed in the center of the "segment", (ii) juxtaposes combinations of biomolecules into well-defined spatial organization, (iii) exerts a controlled tension in the low piconewton (pN) range on the target biomolecule, (iv) isolates biomolecules and maintain their stability in their active state, (v) stabilizes challenging membrane proteins in solution, (vi) provides high flexibility to reach a large variety of orientations important for single-particle imaging, (vii) drives the particles to distribute evenly within a thin ice layer from the cryo-EM grid holes in a variety of orientations, and helps to prevent possible aggregation problems at high particles concentration or from the air-water interface.

In this study, we demonstrate the versatility of our DNA nanostructure as a scaffolding molecular system for a variety of proteins that spans the range of potential targets for single-particle EM. For each application, the binding site is specifically customized to accommodate the protein of interest; either naturally interacting with DNA such as Central glycolytic gene Repressor (CggR), DNA repair Ku70-Ku80 (Ku) heterodimer, and multi-subunit DNA-dependent RNA polymerase (RNAP), or through site specific interactions such as biotin/anti-biotin antibody, bio-tin/streptavidin, or by combining chemical modification of the biotinylated DNA strand of the nanotemplate with specific strep-tagged G protein-coupled receptors (mu-Opioid receptor, μOR). As a proof-of-principle we explored this approach under negative stain conditions for the three-dimensional (3D) reconstruction of the E. coli RNAP holo-enzyme that specifically binds to its nucleic acid target implemented on the DNA nanotemplate. We also demonstrate the compatibility of the design with cryo-EM conditions that can be applied to optimize sample preparation conditions to perform cryo-EM for single-particle collection.

RESULTS

Design of the DNA origami nanotemplate

The overall V-shaped DNA nano-platform design involves the self-assembly of 18-helices at a 140 nm length programmed to globally bend at 60° as depicted in **Figure 1** (also see cadnano diagram of the design in **Figure S1**). The upper bound of the persistence length of the stiff eighteen-helix bundle (18-hb) arm was calculated to be 11.3 μm. A segment of 156 nucleotides

(nt) scaffold connects the two arms of the nanotemplate and is located 45 nm from the kink, such that the distance between the "left" and "right" arms at these points (∼47 nm) is directly mirrored across the nano-template (**Figure 1a** and **Figure S1a**) and able to accommodate large macromolecular complexes up to 47 nm diameter size.

DNA-binding proteins often require the bending of specific DNA strands to facilitate interactions. The structure and kinetics of DNA-binding proteins can be modified when the DNA substrate is subjected to mechanical forces.[23] In our design, the length of the connecting segment can be adjusted by substituting a small number of staple strands, storing the excess scaffold in a reservoir loop on the left end of the template. The number of nt involved in the segment can be adjusted between 84 nt and 156 nt. The length can thus be tuned cost-efficiently with defined and controlled tension in the low pN range, calculated using a modified Freely-Jointed-Chain model (mFJC) as described in Smith SB. et al. study[37] (also see **Supporting Information, SI Elastic response of DNA**).

Extra DNA helix bundle has been designed at one arm extremity to represent a distinct asymmetric and recognizable feature that can be used on electron micrographs to distinguish the orientation of the molecular templates (see schematic 3D design in **Figure 1a** and **Figure S1**). Furthermore, this extra DNA helix bundle can serve as an interface to drive the hierarchical assembly of the monomeric object into oligomerized DNA objects by blunt-end stacking.[36] In this design version, eight-helix bundles are protruding from the "right-arm" of the object to program the self-assembly of two monomers into homodimers. Here, the advantage of using blunt-end stacking is to create a junction between the two monomers with an angular degree of freedom without restricting the range of rotation between the two monomers.[24] The assembling

strategy in this design version will allow imaging multiple viewing angles of the templated particles using the same DNA origami object (**Figure 1b**, and **Figure S2**). The connection occurs in one-pot annealing without intermediate purification steps. Furthermore, to reach maximum viewing orientations of the templated protein-DNA complexes the freedom of rotation of the segment was increased by introducing a single-strand break, or nick[25] at the joint region, connecting the segment to the arms of the V-shape. This loss of base pairing interactions forces the segment helices to deform and allows conformational dynamics within the dsDNA-binding domain. Folding of the nanotemplate in their monomeric form resulted in products that migrate as sharp bands on a 1% native agarose gel electrophoresis (**Figure S1c**). Negative-stain TEM confirmed the assembly of the overall V-shape objects (**Figure 1** and **Figures S3-S5**) with an average bend angle determined to be about 61.4° ± 4.7° (N=144). In this design, the V-shape dimerization assembly proceeds with high yield, as evidenced by a bright band that corresponds to the dimeric V-shape form (**Figure S2b**), clearly recognizable by negative-stained TEM imaging after purification of the dimeric band (**Figure 1b** and **Figure S5**). Mixed populations of dimeric and monomeric origami nanotemplates are often observed under TEM visualization, with a dominant presence of the dimeric forms (**Figure S3**). The dimeric nanostructures present a different range of rotation between the two assembled monomeric forms, as corroborated by direct TEM imaging where the dimeric nanostructures are mainly in "Z-shape" or "U-shape" conformation, and a number of other intermediate states are also visible (**Figure 1b** and **Figure S5**).

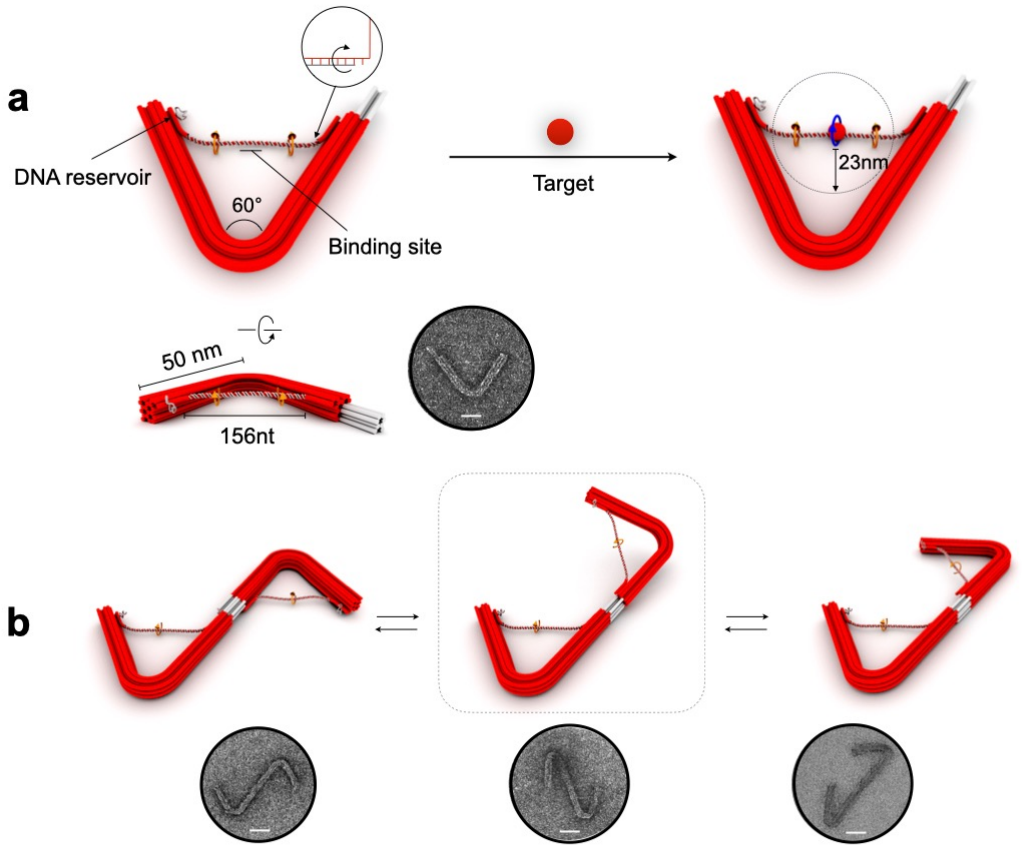

Figure 1. Design of the V-Shape DNA Origami structure. **(a)** Schematic 3D-design of the nanotemplate. The binding site designed for a specific target protein is located at the center of the dsDNA segment connecting the two arms. The length of the segment can be adjusted between 84 nt and 156 nt by storing the excess scaffold in a reservoir loop on the left end of the template and exerting a controlled tension in the low pN range on the target biomolecule. Reducing the number of nucleotides spanning the 46 nm distance gap in-between the two arms leads to a higher structural tension. The dsDNA helix of the segment is designed with a single-strand break at each side to provide the freedom rotation of the connected dsDNA-binding domain. The V-shape nanostructure can hold various sizes of macromolecules, up to ~47 nm in diameter. **(b)** Extra structure, shown in gray at the end of the "right" arm allows the assembly of the

monomeric object into dimer by blunt-end stacking Schematic illustration of the different dimeric assemblies indicate different orientations between two monomers. Examples of TEM micrographs of negatively stained nanotemplates of purified samples in their monomeric and dimeric structures. The connecting segment between the two arms is too thin to be clearly visible in negative stain TEM. Scale bars: 20 nm.

Modularity of the design for versatile applications

We then exploited the nanotemplate to image several biologically relevant proteins. For each target, we engineered the design and/or chemical function of the connecting segment according to the protein of interest, while the rest of the core of the nanostructure was kept unchanged. We prepared three separate pools that contain staples forming the core of the template, the connecting segment, and the reservoir loop. In the following, we highlight the modular properties of the design applied to five different proteins, either interacting spontaneously with DNA, or through site specific conjugation using non-covalent chemical recognition.

Design property I: Customize the three-dimensional shape. DNA-binding protein complexes may require a pre-coupling with a specific dsDNA substrate to retain stability in solution. We explored the ability of the template to accommodate a pre-assembled complex of DNA-protein. In this design version, the single scaffold DNA segment connecting the two arms of the nanotemplate is absent. Instead, two connection sites were introduced for the hybridization of a DNA fragment initially coupled with its protein in-between the platform's empty arms. In addition, the nanotemplate is bearing an extra twelve-helix bundle on the inner side of the "left-arm" (**Figure 2** and **Figure S6** for cadnano design diagram) and can be programmed to self-

assemble into a convex triangle as previously reported.[4] Successful folding of the monomeric template is demonstrated from the characteristic agarose gel bands (**Figures S6b** and **S6c**) and the recognizable purified structure from TEM micrograph (**Figure 2**). As a model, we chose to template the CggR protein-DNA complex. At first, binding of CggR protein (a tetramer of 149 kDa) to its tandem full-length operator site, a DNA sequence of 45-nt, was optimized (see Methods for detailed sequence). To selectively hybridize the tandem full-length operator site into the connection points, we introduced a corresponding 21-nt single strand to the operator site, which has an over-hang at the 3′-side (detailed sequences in **Table S2**). Then, we optimized the hybridization on the nanotemplate by mixing the CggR-DNA complex with the empty DNA origami together at different molecular ratios, (origami:CggR) varying from (1:1) to (1:15), and at different incubation time, from 10 to 60 min (see Methods for more details). In these experiments, fluorescently labeled tandem full-length operator sites were used to monitor the hybridization of the CggR-DNA complex into the template via agarose gel-electrophoretic mobility analysis (**Figure S7b**). We found an optimal hybridization at a molar ratio (CggR-DNA: origami) = (4:1) for 15 minutes at 25 °C. The sample was then loaded onto Superdex S200 10/300 GL column to remove excess free CggR bound protein, and the fractions for the DNA origami-CggR complex were collected and concentrated individually before TEM visualization. The TEM data (**Figure 2** and **Figure S8**) revealed well-dispersed particles with recognizable protein binding features, and demonstrated the accurate fill-up of the empty gap between the two arms.

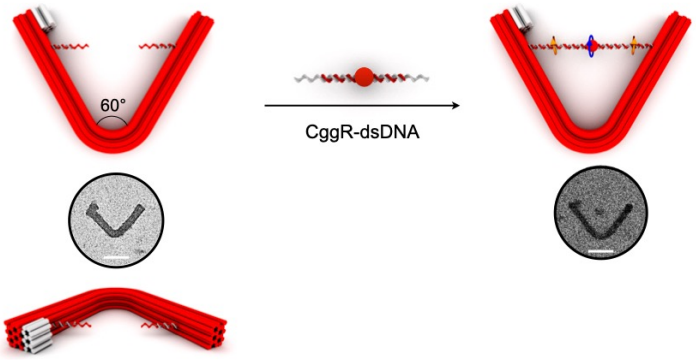

Figure 2. Modular 3D-shape to accommodate pre-assembled DNA-protein complexes. The target CggR protein is coupled by hybridization of the DNA fragment initially templated with the target in between the nanotemplate empty arms. Examples of TEM micrographs of the nanotemplates before and after protein attachment are shown. Scale bars, 20 nm.

Design property II: Tune the spatial molecular organization. Biological functions are often associated with stability and molecular organization of proteins. These functions originate from cooperative and allosteric mechanisms, stabilizing local interactions within a repeat, between adjacent repeats, or at the supramolecular level. Controlling the molecular and spatial organization of proteins is thus very informative but very challenging in structural biology, mainly due to the flexibility of some of these protein complexes that limit their study by crystallography and EM. Here, we investigated Ku protein, which is a heterodimer of two proteins termed Ku70 (70kDa) and Ku80 (80kDa). Ku is a core factor of the main double-strand break (DSB) repair pathway in humans, called non-homologous end-joining (NHEJ).[26, 27] Ku recognizes the DSB ends though its ring shape structure [28] and has a high affinity, in the nanomolar range, for DNA. Beyond its role in the DSB ends recognition, Ku has also a major

role to recruit and orchestrate the function of the NHEJ factor close to DSB ends.[29] Despite preliminary structural studies on Ku complexes with some NHEJ partners or motifs derived from these partners, we have little insight on the way Ku recruits and positions NHEJ enzymes and complexes close to the DSB ends.[30, 31] A limitation of Ku studies by EM is the difficulty to evaluate during sample optimization the proportion of Ku molecules bound to DNA substrates. We evaluated the V-shaped structure to select the Ku-DNA complex in a more efficient way. To this end, ds-DNA fragment of a specific length was designed to control the number of Ku proteins to accommodate. We used two V-shaped DNA origami with a 21 bp or 42 bp double DNA pointing out at the center of the segment connecting the two arms, called Ku (I) and Ku (II), respectively as depicted in **Figure 3**. Ku (I) and Ku (II) nanotemplates allow respectively one or two Ku molecules to bind in the middle of the transverse segment. Indeed, Ku binds DNA in a sequence independent manner. It can thread inside DNA with one Ku molecule bound every 15-20 bp of DNA.[32] In a previous work, we showed by calorimetry that one Ku molecule binds to an 18 bp DNA with a K_d of 3.5 ± 0.8 nM and a 1:1 stoichiometry and that two Ku molecules bind a 42 bp DNA with a K_d of 0.4 ± 0.2 nM and a 2:1 stoichiometry.[30] The presence of Ku proteins at the capturing DNA strand was clearly observed under TEM on both Ku (I) and Ku (II) designs as indicated in **Figure 3** and **Figures S9** and **S10**.

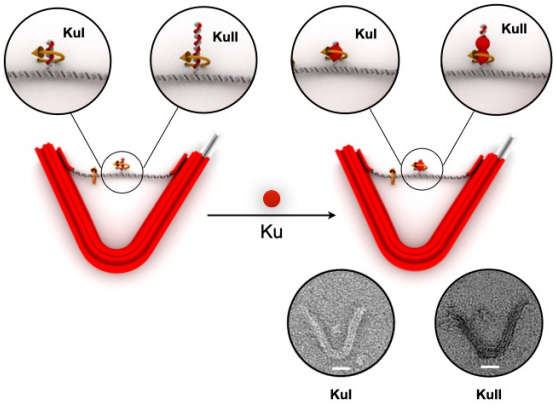

Figure 3. Tunable design for spatial molecular organization. The dsDNA fragment of a specific length is designed to control the number of Ku proteins on the V-shape. Ku (I) and Ku (II) nanotemplates allow respectively one or two Ku particles to bind in the middle of the transverse segment of 21 bp or 42 bp length. Examples of TEM micrographs of the nanotemplates after protein attachment on both designs are shown. Scale bars: 20 nm.

Design property III: Regulate the structural tension of DNA-binding domain. A ssDNA reservoir loop was designed to adjust the number of bases between the fixed empty gap distance between the two arms and thus the contour length of the ssDNA that directly exerts a local tension towards the molecular system by acting as an entropic spring as reported in Philipp C. Nickels et al, study [33] (**Supporting Information, SI Elastic response of DNA** and **Figure S11**).

We studied the force dependency of the RNAP-binding to its core promoter sequence localized in the middle of the dsDNA segment. We regulated the tension by adjusting the length of the ds-DNA segment in the joints of the core promoter sequence. A mismatch-bubble of 9 nt was introduced in the connecting segment to hold the RNAP (~450 kDa)[34] in place of the promoter

region (**Figure 4a**). We investigated low (~ 0 pN) and relatively high (~ 14 pN) force ranges by tuning the length of the dsDNA segment between relaxed (156-nt dsDNA) and tense (134-nt dsDNA) states, respectively (**Figure S12**). The resulting force was calculated for a given contour length by approximating the dsDNA as a semi-flexible polymer[35] and using a mFJC model[36] (**Supporting Information, SI Elastic response of DNA**). The nanotemplates were assembled for each chosen length of the dsDNA connecting segment. After purification, DNA origami 156-nt dsDNA was hybridized with RNAP (see Methods for more details) in an optimized molar ratio of (origami:RNAP)=(1:2). TEM micrographs show the presence of RNAP (**Figure 4**) with a binding efficiency estimated above 70% (from a total number of templates, N= 370) (**Figure S13**). The percentage of templated RNAP particles decreased significantly on the tense 134-nt dsDNA segment at ~ 14 pN, even at higher molar ratio (origami:RNAP) = (1:5) for which the binding efficiency was only ~ 14% (from N= 206) (**Figure S14**). RNAP binds more favorably in the bubble DNA of the relaxed 156-nt dsDNA with a zero-force stress (**Figures S13, S15**, and **S16**). This is consistent with the fact that tense DNA template creates steric constraints impairing RNAP-promoter complex formation and that formation of the RNAP-open promoter complex likely occurs on relaxed dsDNA, inducing ~ 90° bend in DNA as previously estimated from structural studies.[37, 38]

The incorporation of the protein to the DNA nanotemplate drives the isolation of single particles RNAP only coupled to its DNA binding site and serves as a benchmark to facilitate particle selection from the raw micrographs. Particles templated favorably on the relaxed 156-nt dsDNA were thus selected and subjected to 2D class averaging (see Methods, section "Image processing details of negatively stained RNAP"). The density of RNAP in 2D class averages is readily

recognized, with variability in the shape (**Figure 4c**), reflecting different orientations of RNAP in these classes. We then computed a 3D reconstruction of RNAP using Relion software.[39] About 4,000 particles localized in both monomeric and dimeric nanotemplate forms (**Figures S15** and **S16**) were used for final 3D refinement giving a 25Å resolution EM-map. The main structural features of RNAP (**Figure 4c**) agree with the resolved cryo-EM structure of RNAP.[40]

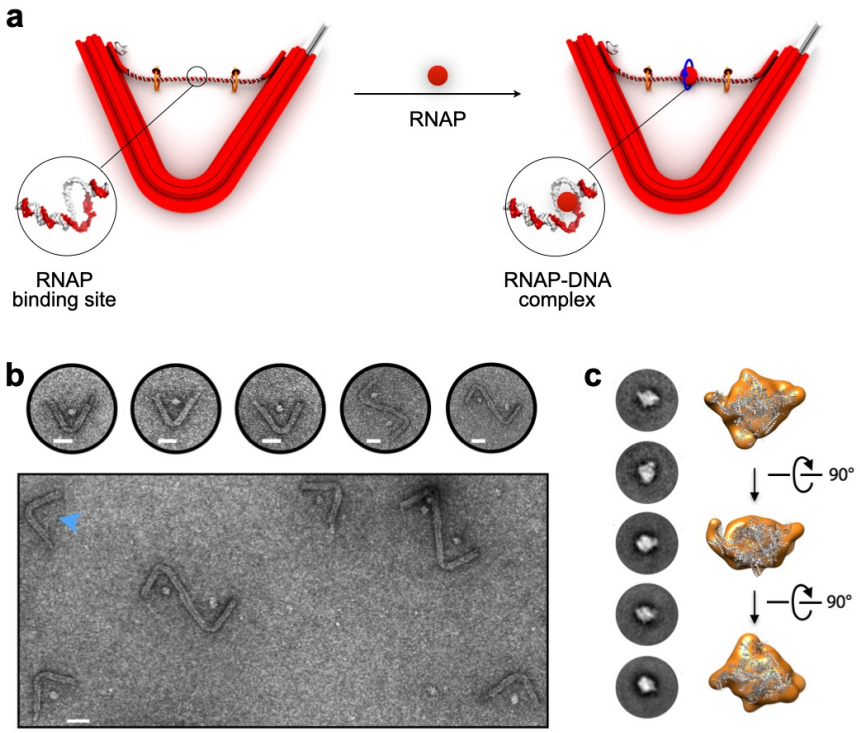

Figure 4. RNAP binding to the relaxed 156-nt dsDNA connecting segment of the V-shape. **(a)** Design of the nanotemplate for RNAP conjugation. The connecting segment is modified with a transcription bubble sequence representing the binding site of the RNAP. **(b)** Representative digital micrograph area of negatively stained DNA origami nanotemplate. Attachment of the RNAP to the binding site results in the appearance of single brighter dots in the center of the

connecting segment of the nanotemplate, indicating successful protein binding in molar ratio of (origami:RNAP) = (1:2). **(c)** Representative 2D class averages and 3D reconstruction of RNAP. The main structural features of RNAP agree with the resolved cryo-EM structure of RNAP in reference 40. Empty DNA origami nanostructures indicated by blue arrow in (b) are discarded from data processing. Scale bars: 40 nm.

Design property IV: Direct site-specific conjugation through chemical modification. To investigate biomolecules other than DNA-binding proteins, we adapted a ligand-receptor binding method through two strategies using biotinylated DNA origami.

First, we explored the applicability of the method using antibiotin-biotin complex, an important class of antibody-antigen interactions commonly used in structural biology.[41] Here, we engineered the nanotemplate with two integrated biotin ligands separated by ~12 nm to simultaneously bind the two antigen-binding sites present at equivalent distance on the anti-biotin, as shown in **Figure 5a**. After coupling optimization and size exclusion chromatography purification, imaging of the purified sample revealed monodisperse particles under negative stain EM, indicating the recognizable antibody feature (**Figure 5a** and **Figure S17**).

Second, we developed a generic method for the study of any arbitrary target protein including membrane proteins. The method relies on the incorporation of a commercially available dual-biotin labeled DNA onto the segment to couple a tetrameric streptavidin protein based on the highly selective recognition of streptavidin to biotinylated DNA. The two free streptavidin binding sites can capture a biotinylated or strep-tagged protein. As a proof-of-concept, we used

the type mu-Opioid receptor (μOR), a G protein-coupled receptor (GPCR). This membrane receptor is a key signaling seven-transmembrane protein that possess important potential in drug discovery programs.[42–44] For attachment to the DNA origami, we genetically engineered the μOR receptor with a twin-strep-tag appended to the carboxy terminus to create a strep-tagged recombinant μOR (see Methods for more details). The strep-tag is a short peptide of 8 amino acids which is able to mimic biotin. The twin-strep-tag is composed of two strep-tag peptide sequences with an internal linker region. Subsequently, the twin-strep-tagged μOR-receptor can be specifically captured via the two free binding sites of the streptavidin attached onto the origami.[45] After PEG-purification of the dual-biotin labelled DNA origami, the sample was mixed with a streptavidin solution. The non-attached streptavidin molecules were separated from the origami by molecular mass cutoff filtration. Finally, the purified origami-streptavidin nanotemplates were incubated with the purified twin-strep-tagged μOR receptor at a molar ratio of (~1:1) of streptavidin to twin-strep-tag μOR receptor, overnight at 4 °C before imaging. The TEM data in **Figure 5b** and **Figure S18** revealed well-dispersed particles with recognizable protein binding features in between the two arms of the nanotemplate.

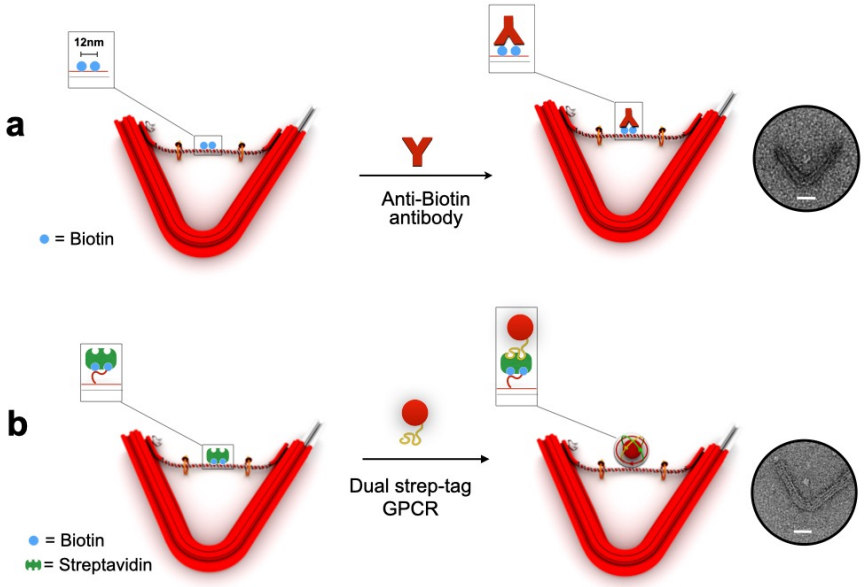

Figure 5. Design of the DNA nanotemplates for specific protein attachment through site specific conjugation. (**a**) Antibiotin-biotin recognition. The connecting segment of the nanotemplate is modified with two integrated biotins ligands separated strategically by ~12 nm to simultaneously bind the Y shaped receptor antibody. (**b**) Specific immobilization of twin-strep-tagged GPCR protein on the bridge segment modified with two biotin molecules, subsequently modified with streptavidin to allow stable immobilization of dual strep-tagged GPCR protein through multivalent attachment, illustrated as anchorage of two strep-tagged sequence to two binding sites of streptavidin. Examples of TEM micrographs of the templated proteins to each specific binding site are shown. Scale bars 40 nm.

Single-particle imaging by Cryo-electron microscopy. Lastly, we tested the compatibility of our V-shape design with cryo-EM sample preparation. To be suitable for cryo-EM sample preparation, the template should be stable at high concentration ranging from 0.5 to 10 μM

required to get enough particles per grid hole. We established a large-scale synthesis and purification strategy of the nanotemplate (see details in Methods). We then optimized sample preparation conditions of the V-shape DNA origami without protein and visualized them on a holey carbon grid at different concentrations. We found conditions where the aqueous suspension of DNA nanotemplates should be concentrated to 0.5 μM (see Methods for estimation of DNA origami concentration) at which the nanostructures are spontaneously embedded in vitreous ice, thereby creating dense, non-overlapping origami nanostructures with multiple orientations, suitable for imaging a target protein by cryo-EM (**Figure 6** and **Figure S19**). For the different tested origami concentrations (i.e., from 0.5 to 10 μM), the nanostructures remain stable and well-dispersed (**Figure 6b**). However, at 10 μM concentration, which is the maximum occupancy in ice, the V-shape templates spontaneously form stable and pseudo ordered 2D-organization structures without aggregation where most of the nanostructures are preferably oriented facing up (**Figure S20**). This preferred orientation might be related to the ssDNA (i.e., poly-thymine nucleotides) added to the extremity of one of the arms to prevent end-to-end polymerization, which probably make them more likely to interact with the hydrophobic air–water interface due to the exposed aromatic bases as previously reported.[13]

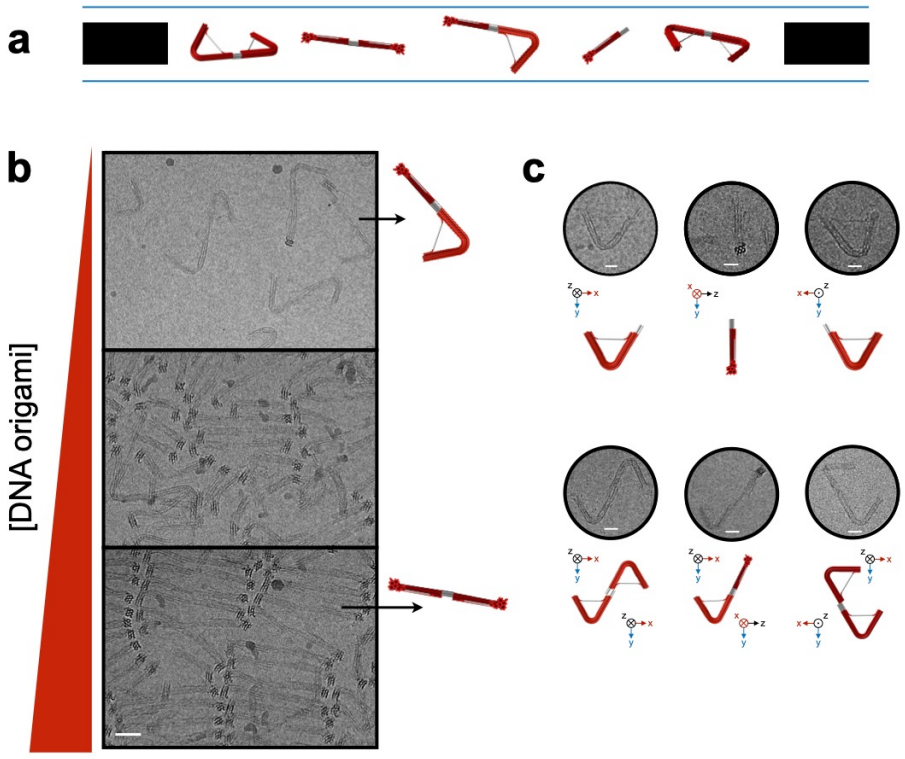

Figure 6. Single-particle imaging by cryo-EM. **(a)** Schematic diagram of grid hole cross-sections containing regions of ideal DNA origami particle for single-particle cryoEM collection. **(b)** Optimization of DNA-origami concentration. Dense and non-overlapping origami nanotemplates with multiple orientations are observed at different concentrations: 0.5; 4; and 10 μM from top to bottom. At the highest concentration, the micrographs show mainly nanotemplates with the two arms facing up and more adopting an orientation perpendicular to the air-water interface. Scale bar, 40 nm. **(c)** Different viewing angles of the nanostructures embedded in vitreous ice. Scale bar, 20 nm.

DNA origami concentration will then be intermediate and was estimated at 0.5 μM. We thus used this concentration to perform cryo-EM imaging on the DNA origami-RNAP complex as proof-

of-principal (**Figure 7**). Purified DNA nanotemplate and concentrated to 0.5 µM were incubated with RNAP in the optimized molar ratio of 1:2 for 30 minutes at 37°C. Direct imaging of the RNAP-origami complex by cryo-EM was clearly observed on the DNA platform. Most of the DNA platforms display isolated RNAP particles (indicated by the red circles in **Figure 7a** and **Figure S21**) and showed suitable contrast in ice. By enclosing RNAP protein in between the two arms of the V-shaped nanotemplate, the protein is kept protected from the air–water interface. In addition, images of RNAP decorated DNA platforms showed a good distribution with multiple orientations (**Figure 6b** and Figures **S19-S21**). All these criteria agree with prerequisites required for cryo-EM to improve the conditions of sample preparation, which is the primary limiting factor for single-particle analysis.

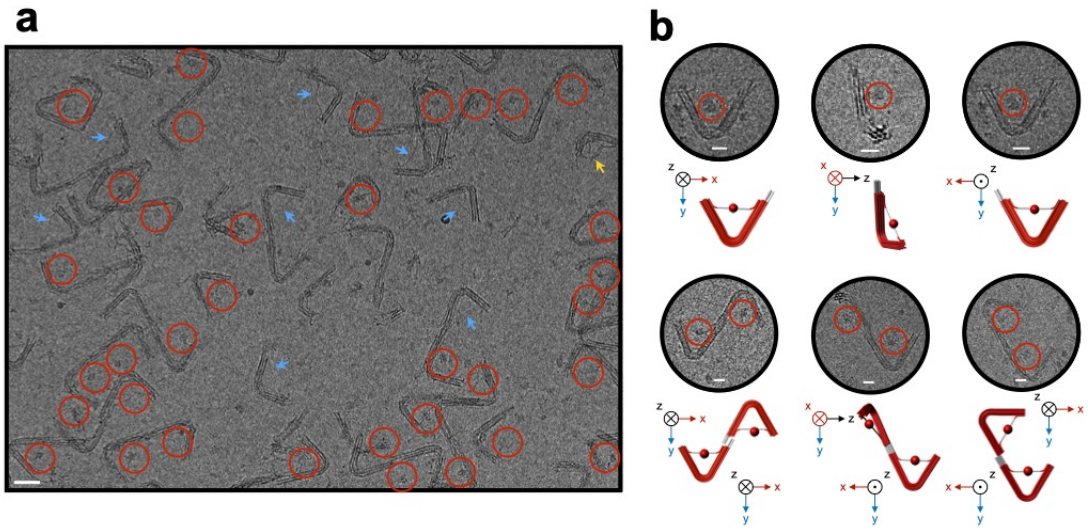

Figure 7. Cryo-electron micrograph of the RNAP coupled to the DNA origami nanotemplate. **(a)** Presence of RNAP to the binding site is indicated by the red circles. Empty DNA origami nanostructures and non-properly folded DNA origami are indicated by blue and yellow arrows, respectively. Scale bar, 40 nm. **(b)** Different viewing angles of the nanostructures-RNAP

embedded in vitreous ice. The presence of RNAP to the binding site is indicated by the red circles. Scale bar, 20 nm.

DISCUSSION

In this study, we present V-shaped DNA origami designs as multifunctional scaffolding molecular systems that help to improve the behavior of the biomolecule for single-particle EM imaging. Sample preparation step is still the primary limiting factor to guarantee the success of the data processing step which is frequently a painstaking trial-and-error process for a large variety of proteins and complexes. For example, DNA- and RNA-binding proteins are difficult to obtain in a homogeneous molecular complex on cryo-EM grids because these complexes often dissociate and DNA/RNA fragments tend to hybridize or aggregate at concentrations required for cryo-EM grid preparation. Similar problems are shared with membrane proteins, wherein it is challenging to obtain a dense distribution of membrane proteins because the hydrophobic particles tend to aggregate. The engineered V-shape structures can help to accomplish the isolation of a variety of target molecules in their active and/or complexed macromolecular states away from the air-water interface and prevents common sample preparation issues. The proposed V-shape design emphasizes two major points.

First, the versatility of coupling of cognate target proteins bound to the DNA origami scaffold are key issues for future studies. Hence, we showed the malleability of the V-shape design to be engineered as desired for five different target proteins, either interacting spontaneously with the DNA or through directed chemical conjugation. The design can be adapted to accommodate DNA-binding protein complexes already pre-coupled to a specific dsDNA substrate in-between

the platform's empty arms as we demonstrated for CggR enzyme. This strategy can be generalized to any DNA-binding protein complexes that may require a pre-coupling with a specific dsDNA substrate to be stable in solution. The design of the DNA present on the center of the origami's segment connecting the two arms can also be engineered without modifying the whole design of the template. We showed the possibility to tune the spatial molecular organization by controlling the number of templated Ku proteins as a function of dsDNA fragment's length. In addition to maintaining stability of the associated molecular complexes that frequently dissociate during the spreading and/or during freezing conditions. This method can be generalized to other proteins interacting with a specific substrate which allows a complete characterization of complex molecular systems at the molecular or supramolecular levels. Our V-shape design can also be programmed to exert a controlled pN force on the molecular system by adjusting the number of nt involved in the segment. We observed that RNAP binds more favourably in the bubble DNA of the relaxed 156-nt dsDNA at ~ 0 pN as compared with the tense 134-nt dsDNA at ~ 14 pN. This is consistent with the fact that DNA binding protein induces DNA structural modifications in general and that gene transcription is a mechano-sensitive process in particular. This strategy may be further adapted to directly visualize other mechano-sensitive molecular systems under tension. In addition, we designed different strategies to study non-DNA binding proteins through site specific conjugation by using commercially available biotin labelled-DNA on the support structure to bind anti-biotin or streptavidin that subsequently can attach streptavidin-tagged target proteins. This functionalization method was adapted to anchor challenging targets such as membrane proteins. The stability of DNA origami over a large selection of detergents and buffers makes the use of DNA origami especially

attractive for structural studies of membrane proteins.[46] Here, we used mu-Opioid receptor (μOR) as an example of GPCR proteins. Our developed method should be easily amenable to other GPCRs which are the largest class of membrane proteins in the human genome. For the different designs, the presence of specific protein or complexes on the center of the V-shaped origami is a guarantee that the interaction between the target and the DNA or RNA is effective as observed on the EM grids.

Second, the scaffolding system was demonstrated to be compatible with cryo-EM conditions. We found conditions where the DNA nanotemplates are spontaneously embedded in vitreous ice, thereby creating dense, non-overlapping origami molecules, and showing different orientations, suitable for imaging target proteins by cryo-EM. As a proof-of-principle, we chose to template RNAP protein that binds favorably to its relaxed core promoter sequence localized in the middle of the 156-nt dsDNA segment at ~ 0 pN.

The DNA origami which is at least one or two orders magnitude more massive than the protein target helps to drive the particles enclosed in the center of the DNA template to distribute evenly within the ice layer of the grid holes in a variety of orientations, as well as permitting facile viewing of different angles of the target protein. In addition, the different orientations of the nanotemplate help to keep the protein target away from the detrimental effects of the air–water interface and can assist in the selection of suitable particles on its DNA binding site. The template can also help to prevent aggregation of the target protein at concentrations needed to perform cryo-EM.

CONCLUSIONS

This study set out to explore a simple, versatile and straightforward method to enable accurate molecular scale positioning as a fiducial marker. These V-shaped DNA origami nanotemplates open the way to juxtapose combinations of several biomolecules into complex arrangements or the regulation of the structural tension imposed by the nanotemplate to control binding affinity which can be visualized by single-particle EM. These scaffolding approaches could provide a distinct opportunity that may inspire future studies on target proteins difficult-to-crystallize or difficult-to-image under cryo-EM conditions. Especially protein complexes and membrane proteins which are inherently difficult to study by cryo-EM because of their instability and tendency to aggregate when extracted from their natural lipid-bilayer environment, particularly for GPCRs.

METHODS

Design and preparation of DNA origami

V-shaped DNA origami structures were designed using CaDNAno software (v. 2.0) using a 7560-nt M13 bacteriophage genome as scaffold. Oligonucleotide staple strands (Eurofins, France) were combined with the 7560-nt scaffold in a one-pot reaction at a ten-fold molar excess in buffer containing 5mM Tris-HCl, pH=7.8, 1mM EDTA, and 18mM $MgCl_2$. The reaction was then heated to 65 °C for 15 minutes to denature all DNA strands, then slowly cooled in a gradient from 60 °C to 40 °C over a 40-hour time span to anneal and assemble the nanostructure. After the folding of the nanostructure the V-shape was analyzed by 1% agarose gel and 0.5X TBE buffer with 11mM $MgCl_2$. Bands corresponding to the DNA origami were excised and purified using DNA gel extraction spin column (Merck, France) centrifuged at 5,000 g for 3 min at 4℃.

Proper folding of the DNA origami was assessed by negative staining with 1% uranyl acetate and visualization by electron microscopy using a JEOL 2200, 200 KeV.

Purification strategy of DNA origami

DNA origami nanostructures were purified from the excess of the oligonucleotide staple strands by separation on 1% agarose gel with 0.5x TBE buffer infused with 11mM $MgCl_2$. Alternatively, nanostructures were purified using at least three rounds of PEG precipitation. Briefly, a solution of 15% w/v PEG-8000 5mM Tris-HCl, pH=7.8, 505mM NaCl, 1mM EDTA was added at equivalent volumes to a sample of DNA origami and centrifuged at 16000xg for 25 minutes at 8°C. Supernatant was removed and the pellet was resuspended in a buffer consisting of 5mM Tris-HCl, 5mM NaCl, 1mM EDTA, 11mM $MgCl_2$. A third strategy to purify V-shape nanostructures consisted of centrifugation of the folded origami in a 100K MWCO amicon centrifugal filter (Merck, France) to concentrate the DNA origami and remove excess oligonucleotide staples. Origami were thoroughly rinsed in this manner with at least six rinses.

Concentration of DNA origami

DNA origami concentration was estimated by measuring DNA absorbance at 260 nm, and applying the Beer-Lambert relation. We then used the formula for the extinction coefficient $\varepsilon = 6700Nds + 10000Nss$, wherein the Nds and Nss are of double stranded and single stranded nucleotides, respectively.[47] Final DNA concentration varied according to the purification strategy, typically between 10 nM and 20 nM using centrifugal filters and between 0,5 µM - 5 µM using PEG precipitation method. The absorbance was measured using a nanodrop UV-vis spectrophotometer (Thermo scientific, France).

Expression and purification of target proteins

CggR protein. The CggR/DNA complex was purified as described in Chaix et al.[48] using a dsDNA oligonucleotide containing the tandem full-length operator site (45-nt, 5'-TGACGGGACGTTTTTTGTCATAGCGGGACATATAATGTCCAGCAA-3'). The assembly of the CggR nanotemplate was accomplished in a similar manner as the nanotemplate version 2, in the presence of six equivalents of the capturing strands. After PEG-purification, purified DNA origami sample was mixed with the CggR protein bound to the tandem full-length operator site at different molecular ratio, varying from 1:1 to 1:15, origami:CggR and incubation time, from 10 to 60 min. The resulting DNA origami/CggR conjugates were purified by size-exclusion chromatography. The samples were loaded onto Superdex S200 10/300 GL column to remove excess free CggR bound protein, and the fractions for the DNA origami-CggR complex were collected and concentrated individually before TEM visualization.

Ku protein. The full-length human Ku70 (1–609)/Ku80 (1–732) heterodimer was prepared as previously described.[49] Briefly Ku70/80 was cloned in the Multibac vectors with a 10-His tag and a tobacco etc h virus (TEV) site on the Ku80 N-terminus. The plasmid was integrated in a yellow fluorescent protein-containing bacmid by transformation in EMBACY Escherichia coli stain (kind gift from I Berger, Bristol University). The resulting recombinant bacmids were used to transfect Sf21 insect cells, giving the V0 virus generation. Production was initiated in Sf21 cell culture by infection with baculovirus at a multiplicity of infection (MOI) of 5×10^{-3}. Insect

cells were collected 5–6 days after the infection (3–4 days after the proliferation arrest). The Ku heterodimer was purified on an Ni NTA-Agarose affinity column (Protino, Macherey Nagel) with a 1M NaCl wash step to remove DNA excess. The eluted Ku was then bound onto an anion exchange column (Resource Q, GE Healthcare) equilibrated with buffer Q (20 mM Tris pH 8.0, 50 mM NaCl, 50 mM KCl, 10 mM β -mercaptoethanol). Final yield of the Ku heterodimer was typically 35 mg purified heterodimer per liter of culture. For protein attachment to the nanotemplate, Ku heterodimer stored in 50% glycerol was diluted in 10mM Tris pH 8.0, 50 mM NaCl to a final concentration of 75 nM. 0,8µL of diluted Ku was mixed with 4,2µL of purified Ku(I) or Ku(II) nanotemplates at about 20 nM and incubated for less than one minute at room temperature before TEM imaging.

E. coli RNAP holoenzyme. The E. coli RNAP holoenzyme was assembled from the RNAP core and the σ70 subunit expressed and purified as described in Morichaud et al.[50] Annealed DNA structures in presence of six equivalents of RNAP connecting segment staples (5'-AATCATGGTCATAGCTGTTTCCTGTGTGAAATTGTTATCCGCTCACAATTCCACACATTATACGAGCCGGAAGCATAAAGTGTCAAGCCTGGGGTGCCTAATGA-3') were purified by PEG-purification method. Purified E. coli RNAP holoenzyme was assembled to the purified nanotemplate with an optimized molar ratio of (origami:RNAP)=(1:2) for 30 minutes at 37°C, with buffer (10mM Tris pH 8.0, 100 mM NaCl, 5 mM $MgCl_2$).

Antibody, anti-biotin. Annealed DNA structures in presence of six equivalents of Biotin-TEG-labelled staples were purified by 2% agarose gel electrophoresis. HPLC purified DNA sequence modified with Biotin-TEG were obtained from Eurofins, 5'-Biot-TEG-

AGCCGGAAGCATAAAGTGTAA-TEG-Biot-TEG-3'. Purified Biotin-TEG-labelled origami was incubated with the antibody at a molecular ratio of 1:5 for 30 min at 25 °C. Antibody was purchased from Sigma-Aldrich, USA (Anti-Biotin antibody produced in goat, ref: B3640-1MG). The resulting DNA origami/antibody was loaded onto Superdex S200 10/300 GL column to remove excess free antibody, and the fractions for the DNA origami-antibody complex were collected and concentrated individually before TEM visualization.

μ-Opioid Receptor. The mouse μ-Opioid Receptor was prepared as previously described.[51] Briefly, a tobacco etch virus (TEV) protease recognition site was introduced after residue 51, and a human rhinovirus 3C (HRV-3C) protease site after residue 398. A FLAG tag was added to the amino terminus and a Twin-Strep-tag® was appended to the carboxy terminus (μOR-Cter) after the HRV-3C site. Sequence used for the Twin-Strep-tag® (WSHPQFEKGGGSGGGSGGSSAWSHPQFEK, IBA-lifesciences). Recombinant baculoviruses were generated using the pFastBac baculovirus system according to manufacturer's instructions (ThermoFischer). High titer baculoviruses encoding μOR-Cter genes were used to infect Sf9 cells at a cell density of 4×10^6 cells per ml in suspension in media (Sigma Aldrich) in the presence of 3 μM naloxone. Cells were harvested by centrifugation 48 h post-infection and stored at -80 °C until purification. Cell pellets were resuspended in 10 mM Tris-HCl (pH 7.5), 1 mM EDTA buffer containing 2 $mg.ml^{-1}$ iodoacetamide and protease inhibitors without salt to lyse the cells by hypotonic lysis. Lysed cells were centrifuged (38,420 g) and the membranes were solubilized during 1h @ 4 °C using buffer containing 20 mM HEPES (pH 7.5), 200 mM NaCl, 0.5% (w/v) n-dodecyl--D-maltoside (DDM, Anatrace), 0.3% (w/v) CHAPS, 0.03% (w/v) choslesteryl-hemi-succinate (CHS, Sigma), 2 $mg.ml^{-1}$ iodoacetamide and protease inhibitors. The

solubilized receptor was loaded onto anti-Flag M1 column and washed thoroughly with DDM buffer containing 20 mM HEPES (pH 7.5), 100 mM NaCl, 0.1% (w/v) DDM, 0.03% (w/v) CHAPS, 0.015% (w/v) CHS and 2 mM $CaCl_2$. While on the M1 antibody resin, the receptor was exchanged into lauryl-maltose-neopentyl-glycol (MNG-14, Anatrace) detergent-containing buffer composed of 20 mM HEPES (pH 7.5), 100 mM NaCl, 0.5% (w/v) MNG-14 and 0.01 % CHS. The column was then washed with 20x critical micelle concentration (cmc) MNG-14 buffer containing 20 mM HEPES (pH 7.4), 100 mM NaCl, 0.02% (w/v) MNG and 0.0004 % CHS and the bound receptor was eluted in the same buffer supplemented with 0.2 mg.ml-1 Flag peptide. The sample was incubated at 4 °C overnight in the presence of 100 µM of TCEP and TEV at a 1:5: µOR ratio by weight to remove the amino termini. µOR-Cter was further purified by SEC chromatography in a buffer containing 0.01% MNG, 0.001% CHS, 20 mM HEPES pH 7.4 and 100 mM NaCl.

For protein attachment to the nanotemplate. First, the assembly of the dual-tagged nanotemplate was accomplished in a similar manner as the nanotemplate in presence of six equivalents of dual-biotin labelled staples 5'-dual-Biot-TTTCACAATTCCACACAACATACGAGCC-3', (IDT, Modification Code: /52-Bio/). The resulting dual-biot/DNA origami conjugates were purified by PEG-purification method. PEG-purified DNA origami sample was mixed with streptavidin solution (in 20 mM HEPES buffer at pH 7.5 with 100 mM NaCl and10 mM $MgCl_2$) at equal volume to a final concentration of ~80 and 16 nM between DNA origami and streptavidin, respectively. Non-attached streptavidin molecules were removed from the origami nanotemplate by three rounds of molecular mass cutoff filtration by using 100 kDa amicon filters (Millipore) in a buffer (20 mM HEPES at pH 7.5, 100 mM NaCl, and10 mM $MgCl_2$). The purified origami-

streptavidin nanotemplates were then mixed with the purified twin strep-tagged μOR receptor to a final concentration of ~ 14 and 11 nM, the streptavidin and twin strep-tagged μOR receptor in a buffer (20 mM HEPES at pH 7.5, 100 mM NaCl, and10 mM $MgCl_2$). The mixture was incubated overnight at 4 °C before deposition on carbon grid.

Transmission Electron Microscopy Imaging

For imaging in negative stain, 3 μL of the sample was deposited for 2 min onto a glow-discharged carbon-coated grids (Quantifoil Micro tools GmbH, Germany), stained with for 60 s with a 2% (w/vol) aqueous uranyl acetate (Merck, France) solution, and then dried with ashless filter paper (VWR, France). For cryo-EM experiments, 3 μL of samples were applied to glow-discharged Quantifoil R 2/2 grids (Quantifoil Micro tools GmbH, Germany), blotted for 1s and then flash frozen in liquid ethane using the semi-automated plunge freezing device CP3 (Gatan inc.) at 95% relative humidity. All observations of EM-grids were carried out on a JEOL 2200FS FEG operating at 200 kV equipped with a 4k x 4k slow-scan CDD camera (Gatan inc.) under low-dose conditions (total dose of 20 electrons/$Å^2$) in the zero-energy-loss mode with a slit width of 20 eV. Images were taken at a nominal magnification of 50,000 X, with defocus ranging from 0.6 to 2.5 μm. Magnification was calibrated from cryo-images of tobacco mosaic virus.

Image processing of negatively stained RNAP particles

More than 700 images of negatively stained RNAP complexes were checked for drift or astigmatism and RNAP particles extracted semi-automatically using e2eval image and e2boxer respectively, from the Eman2 package.[52] Mainly due to drift, 674 images were used for subsequent image processing.

Two-dimensional class averages were computed using IMAGIC V software[53] according to the method presented in Bron et al,.[54] Briefly, the phase-contrast-transfer function was corrected by phase flipping using defocus parameters obtained using Gctf.[55] A total of 5,846 particles were then grouped into classes and averaged using the MSA (multi-statistical alignment) procedure. The best class averages were then used as references to perform an MRA (multi-reference-alignment) followed by a new MSA. Four alignment cycles were needed to obtain stable 2D class averages.

For three-dimensional reconstruction, we used RELION-3 software.[56] Particles were extracted, normalized, reduced by a factor two giving a pixel size of 4.6Å, and subjected to a 3D classification into four classes. As 2D class averages computed from IMAGIC revealed common structural features with E. Coli RNAP, we used the envelope of E. Coli RNAP (pdb 4YLN) filtered at 60Å as a reference. From the first 3D class, 4,406 particles were selected and used for a 2D classification. The best classes were then subjected to a 3D auto-refine step yielding a final reconstruction at 25Å resolution. Surface representations of the EM-map was performed using Chimera software.[57]

ASSOCIATED CONTENT

Supporting Information Available: Design and characterization of DNA origami structures as well as additional TEM images of the different protein attachments to DNA origami binding sites. The model applied to estimate the force generated on the RNAP-DNA binding domain. And list of all oligonucleotides. This material is available free of charge via the Internet at http://pubs.acs.org.

AUTHOR INFORMATION

Corresponding Author

Gaetan Bellot, E-mail: gaetan.bellot@cbs.cnrs.fr

Patrick Bron, E-mail: patrick.bron@cbs.cnrs.fr

Virginie Ropars, virginie.ropars@i2bc.paris-saclay.fr

Author Contributions

N.A designed and performed the experiments, analyzed the data and wrote the manuscript. J.L.-K.-H performed the electron microscopy experiments. A.M performed the experiments, analyzed the data and wrote the manuscript. N.D purified CggR protein. Z.M and K.B purified RNAP. K.B participated in RNAP experimental design, RNAP data analysis and writing of the manuscript. S.B and E.L.C performed the electron microscopy experiments on Ku protein. J.B.C and V.R designed and supervised the electron microscopy study on Ku protein, interpreted data and wrote the manuscript. R.S and S.G purified mu-Opioid receptor. P.B designed and performed the electron microscopy experiments, computed the 3D reconstruction of RNAP and wrote the paper. G.B conceived, designed and supervised the study, interpreted the data and wrote the manuscript.

Notes

The authors declare no competing financial interest.

ACKNOWLEDGMENT

Research was supported by a French National Research Agency Grant to G.B. (ANR-16-CE09-0004-01) and a labex EpiGenMed fund to G.B. and by an ARC funding, PJA 20171206409 fund to V.R. The CBS is a member of the French Infrastructure for Integrated Structural Biology (FRISBI), a national infrastructure supported by the French National Research Agency (ANR-10-INBS-05).

REFERENCES

(1) Douglas, S. M.; Dietz, H.; Liedl, T.; Högberg, B.; Graf, F.; Shih, W. M. Self-Assembly of DNA into Nanoscale Three-Dimensional Shapes. *Nature* **2009**, *459*, 414.

(2) Wagenbauer, K. F.; Sigl, C.; Dietz, H. Gigadalton-Scale Shape-Programmable DNA Assemblies. *Nature* **2017**, *552*, 78.

(3) Ong, L. L.; Hanikel, N.; Yaghi, O. K.; Grun, C.; Strauss, M. T.; Bron, P.; Lai-Kee-Him, J.; Schueder, F.; Wang, B.; Wang, P.; et al. Programmable Self-Assembly of Three-Dimensional Nanostructures from 10,000 Unique Components. *Nature* **2017**, *552*, 72.

(4) Dietz, H.; Douglas, S. M.; Shih, W. M. Folding DNA into Twisted and Curved Nanoscale Shapes. *Science* **2009**, *325*, 725– 730.

(5) Ke, Y.; Bellot, G.; Voigt, N. V; Fradkov, E.; Shih, W. M. Two Design Strategies for Enhancement of Multilayer-DNA-Origami Folding: Underwinding for Specific Intercalator Rescue and Staple-Break Positioning. *Chem. Sci.* **2012**, *3*, 2587–2597.

(6) Aissaoui, N.; Moth-Poulsen, K.; Käll, M.; Johansson, P.; Wilhelmsson, L. M.; Albinsson, B. FRET Enhancement Close to Gold Nanoparticles Positioned in DNA Origami Constructs. *Nanoscale* **2017**, *9*, 673–683.

(7) Funke, J. J.; Dietz, H. Placing Molecules with Bohr Radius Resolution Using DNA Origami. *Nat. Nanotechnol.* **2015**, *11*, 47.

(8) Tan, S. J.; Campolongo, M. J.; Luo, D.; Cheng, W. Building Plasmonic Nanostructures with DNA. *Nat. Nanotechnol.* **2011**, *6*, 268.

(9) Douglas, S. M.; Bachelet, I.; Church, G. M. A Logic-Gated Nanorobot for Targeted Transport of Molecular Payloads. *Science* **2012**, *335*, 831– 834.

(10) Zhang, Z.; Yang, Y.; Pincet, F.; Llaguno, M. C.; Lin, C. Placing and Shaping Liposomes with Reconfigurable DNA Nanocages. *Nat. Chem.* **2017**, *9*, 653.

(11) Ketterer, P.; Ananth, A. N.; Laman Trip, D. S.; Mishra, A.; Bertosin, E.; Ganji, M.; van der Torre, J.; Onck, P.; Dietz, H.; Dekker, C. DNA Origami Scaffold for Studying Intrinsically Disordered Proteins of the Nuclear Pore Complex. *Nat. Commun.* **2018**, *9*, 902.

(12) Selmi, D. N.; Adamson, R. J.; Attrill, H.; Goddard, A. D.; Gilbert, R. J. C.; Watts, A.; Turberfield, A. J. DNA-Templated Protein Arrays for Single-Molecule Imaging. *Nano Lett.* **2011**, *11*, 657–660.

(13) Martin, T. G.; Bharat, T. A. M.; Joerger, A. C.; Bai, X.; Praetorius, F.; Fersht, A. R.; Dietz, H.; Scheres, S. H. W. Design of a Molecular Support for Cryo-EM Structure Determination. *Proc. Natl. Acad. Sci. USA*. **2016**, *113*, E7456.

(14) Skiniotis, G.; Southworth, D. R. Single-Particle Cryo-Electron Microscopy of Macromolecular Complexes. *Reprod. Syst. Sex. Disord.* **2016**, *6*, 9–22.

(15) Nogales, E. The Development of Cryo-EM into a Mainstream Structural Biology Technique. *Nat. Methods* **2016**, *13*, 24–27.

(16) Noble, A. J.; Dandey, V. P.; Wei, H.; Brasch, J.; Chase, J.; Acharya, P.; Tan, Y. Z.; Zhang, Z.; Kim, L. Y.; Scapin, G.; et al. Routine Single Particle CryoEM Sample and Grid Characterization by Tomography. *Elife* **2018**, *7*, e34257.

(17) Glaeser, R. M. Proteins, Interfaces, and Cryo-EM Grids. *Curr. Opin. Colloid Interface Sci.* **2018**, *34*, 1–8.

(18) Glaeser, R. M.; Han, B.-G. Opinion: Hazards Faced by Macromolecules When Confined to Thin Aqueous Films. *Biophys. reports* **2017**, *3*, 1–7.

(19) Gunning, P. A.; Mackie, A. R.; Gunning, A. P.; Woodward, N. C.; Wilde, P. J.; Morris, V. J. Effect of Surfactant Type on Surfactant−Protein Interactions at the Air−Water Interface. *Biomacromolecules* **2004**, *5*, 984–991.

(20) Stanimirova, R. D.; Marinova, K. G.; Danov, K. D.; Kralchevsky, P. A.; Basheva, E. S.; Stoyanov, S. D.; Pelan, E. G. Competitive Adsorption of the Protein Hydrophobin and an Ionic Surfactant: Parallel vs Sequential Adsorption and Dilatational Rheology. *Colloids Surfaces A Physicochem. Eng. Asp.* **2014**, *457*, 307–317.

(21) Vinothkumar, K. R.; Henderson, R. Single Particle Electron Cryomicroscopy: Trends, Issues and Future Perspective. *Q. Rev. Biophys.* **2016**, *49*, e13.

(22) Noble, A. J.; Wei, H.; Dandey, V. P.; Zhang, Z.; Tan, Y. Z.; Potter, C. S.; Carragher, B. Reducing Effects of Particle Adsorption to the Air–Water Interface in Cryo-EM. *Nat. Methods* **2018**, *15*, 793–795.

(23) Meng, C. A.; Fazal, F. M.; Block, S. M. Real-Time Observation of Polymerase-Promoter Contact Remodeling during Transcription Initiation. *Nat. Commun.* **2017**, *8*, 1178.

(24) Wagenbauer, K. F.; Engelhardt, F. A. S.; Stahl, E.; Hechtl, V. K.; Stömmer, P.; Seebacher, F.; Meregalli, L.; Ketterer, P.; Gerling, T.; Dietz, H. How We Make DNA Origami. *ChemBioChem* **2017**, *18*, 1873–1885.

(25) Lee, C.; Lee, J. Y.; Kim, D.-N. Polymorphic Design of DNA Origami Structures through Mechanical Control of Modular Components. *Nat. Commun.* **2017**, *8*, 2067.

(26) Wang, Y.; Ghosh, G.; Hendrickson, E. A. Ku86 Represses Lethal Telomere Deletion Events in Human Somatic Cells. *Proc. Natl. Acad. Sci. USA.* **2009**, *106*, 12430.

(27) Myung, K.; Ghosh, G.; Fattah, F. J.; Li, G.; Kim, H.; Dutia, A.; Pak, E.; Smith, S.; Hendrickson, E. A. Regulation of Telomere Length and Suppression of Genomic Instability in Human Somatic Cells by Ku86. *Mol. Cell. Biol. USA.* **2004**, *24*, 5050.

(28) Walker, J. R.; Corpina, R. A.; Goldberg, J. Structure of the Ku Heterodimer Bound to DNA and Its Implications for Double-Strand Break Repair. *Nature* **2001**, *412*, 607.

(29) Frit, P.; Ropars, V.; Modesti, M.; Charbonnier, J. B.; Calsou, P. Plugged into the Ku-DNA Hub: The NHEJ Network. *Prog. Biophys. Mol. Biol.* **2019,** 147, 62-76.

(30) Nemoz, C.; Ropars, V.; Frit, P.; Gontier, A.; Drevet, P.; Yu, J.; Guerois, R.; Pitois, A.; Comte, A.; Delteil, C.; et al. XLF and APLF Bind Ku80 at Two Remote Sites to Ensure DNA Repair by Non-Homologous End Joining. *Nat. Struct. Mol. Biol.* **2018**, *25*, 971–980.

(31) Hnízda, A.; Blundell, T. L. Multicomponent Assemblies in DNA-Double-Strand Break Repair by NHEJ. *Curr. Opin. Struct. Biol.* **2019**, *55*, 154–160.

(32) de Vries, E.; van Driel, W.; Bergsma, W. G.; Arnberg, A. C.; van der Vliet, P. C. HeLa Nuclear Protein Recognizing DNA Termini and Translocating on DNA Forming a Regular DNA-Multimeric Protein Complex. *J. Mol. Biol.* **1989**, *208*, 65–78.

(33) Nickels, P. C.; Wünsch, B.; Holzmeister, P.; Bae, W.; Kneer, L. M.; Grohmann, D.; Tinnefeld, P.; Liedl, T. Molecular Force Spectroscopy with a DNA Origami-Based Nanoscopic Force Clamp. *Science* **2016**, *354*, 305–307.

(34) Finn, R. D.; Orlova, E. V; Gowen, B.; Buck, M.; van Heel, M. Escherichia Coli RNA Polymerase Core and Holoenzyme Structures. *EMBO J.* **2000**, *19*, 6833–6844.

(35) Shusterman, R.; Alon, S.; Gavrinyov, T.; Krichevsky, O. Monomer Dynamics in Double- and Single-Stranded DNA Polymers. *Phys. Rev. Lett.* **2004**, *92*, 48303.

(36) Smith, S. B.; Cui, Y.; Bustamante, C. Overstretching B-DNA: The Elastic Response of Individual Double-Stranded and Single-Stranded DNA Molecules. *Science* **1996**, *271*, 795–799.

(37) Feklistov, A.; Bae, B.; Hauver, J.; Lass-Napiorkowska, A.; Kalesse, M.; Glaus, F.; Altmann, K.-H.; Heyduk, T.; Landick, R.; Darst, S. A. RNA Polymerase Motions during Promoter Melting. *Science* **2017**, *356*, 863–866.

(38) Zuo, Y.; Steitz, T. A. Crystal Structures of the E. Coli Transcription Initiation Complexes with a Complete Bubble. *Mol. Cell* **2015**, *58*, 534–540.

(39) Zivanov, J.; Nakane, T.; Forsberg, B.; Kimanius, D.; Hagen, W. J. H.; Lindahl, E.; Scheres, S. H. W. RELION-3: New Tools for Automated High-Resolution Cryo-EM Structure Determination. *bioRxiv* **2018**, 421123.

(40) Narayanan, A.; Vago, F. S.; Li, K.; Qayyum, M. Z.; Yernool, D.; Jiang, W.; Murakami, K. S. Cryo-EM Structure of Escherichia Coli σ(70) RNA Polymerase and Promoter DNA Complex Revealed a Role of σ Non-Conserved Region during the Open Complex Formation. *J. Biol. Chem.* **2018**, *293*, 7367–7375.

(41) Khoo, M. M.; Ng, K. L.; Alias, Y.; Khor, S. M. Impedimetric Biotin—Immunosensor with Excellent Analytical Performance for Real Sample Analysis. *J. Electroanal. Chem.* **2017**, *799*, 111–121.

(42) Sounier, R.; Mas, C.; Steyaert, J.; Laeremans, T.; Manglik, A.; Huang, W.; Kobilka, B. K.; Déméné, H.; Granier, S. Propagation of Conformational Changes during μ-Opioid Receptor Activation. *Nature* **2015**, *524*, 375–378.

(43) Matthes, H. W. D.; Maldonado, R.; Simonin, F.; Valverde, O.; Slowe, S.; Kitchen, I.; Befort, K.; Dierich, A.; Le Meur, M.; Dollé, P.; et al. Loss of Morphine-Induced Analgesia, Reward Effect and Withdrawal Symptoms in Mice Lacking the μ-Opioid-Receptor Gene. *Nature* **1996**, *383*, 819–823.

(44) Macht, D. I.; Herman, N. B.; Levy, C. S. A Quantitative Study of Cutaneous Analgesia Produced by Various Opium Alkaloids. *Proc. Natl. Acad. Sci. USA*. **1915**, *1*, 582.

(45) Schmidt, T. G. M.; Koepke, J.; Frank, R.; Skerra, A. Molecular Interaction Between the Strep-Tag Affinity Peptide and Its Cognate Target, Streptavidin. *J. Mol. Biol.* **1996**, *255*, 753.

(46) Bellot, G.; McClintock, M. A.; Chou, J. J.; Shih, W. M. DNA Nanotubes for NMR Structure Determination of Membrane Proteins. *Nat. Protoc.* **2013**, *8*, 755.

(47) Hung, A. M.; Micheel, C. M.; Bozano, L. D.; Osterbur, L. W.; Wallraff, G. M.; Cha, J. N. Large-Area Spatially Ordered Arrays of Gold Nanoparticles Directed by Lithographically Confined DNA Origami. Nat. Nanotechnol. **2010**, 5, 121–126.

(48) Chaix, D.; Ferguson, M. L.; Atmanene, C.; Van Dorsselaer, A.; Sanglier-Cianférani, S.; Royer, C. A.; Declerck, N. Physical Basis of the Inducer-Dependent Cooperativity of the Central Glycolytic Genes Repressor/DNA Complex. Nucleic Acids Res. **2010**, 38, 5944–5957.

(49) Nemoz, C.; Ropars, V.; Frit, P.; Gontier, A.; Drevet, P.; Yu, J.; Guerois, R.; Pitois, A.; Comte, A.; Delteil, C.; et al. XLF and APLF Bind Ku80 at Two Remote Sites to Ensure DNA Repair by Non-Homologous End Joining. Nat. Struct. Mol. Biol. **2018**, 25, 971–980.

(50) Morichaud, Z.; Chaloin, L.; Brodolin, K. Regions 1.2 and 3.2 of the RNA Polymerase σ Subunit Promote DNA Melting and Attenuate Action of the Antibiotic Lipiarmycin. J. Mol. Biol. **2016**, 428, 463–476.

(51) Sounier, R.; Mas, C.; Steyaert, J.; Laeremans, T.; Manglik, A.; Huang, W.; Kobilka, B. K.; Déméné, H.; Granier, S. Propagation of Conformational Changes during μ-Opioid Receptor Activation. Nature **2015**, 524, 375–378.

(52) Tang, G.; Peng, L.; Baldwin, P. R.; Mann, D. S.; Jiang, W.; Rees, I.; Ludtke, S. J. EMAN2: An Extensible Image Processing Suite for Electron Microscopy. J. Struct. Biol. **2007**, 157, 38–46.

(53) van Heel, M.; Harauz, G.; Orlova, E. V; Schmidt, R.; Schatz, M. A New Generation of the IMAGIC Image Processing System. J. Struct. Biol. **1996**, 116, 17–24.

(54) Bron, P.; Giudice, E.; Rolland, J.-P.; Buey, R. M.; Barbier, P.; Díaz, J. F.; Peyrot, V.; Thomas, D.; Garnier, C. Apo-Hsp90 Coexists in Two Open Conformational States in Solution. Biol. Cell **2008**, 100, 413–425.

(55) Zhang, K. Gctf: Real-Time CTF Determination and Correction. J. Struct. Biol. **2016**, 193, 1–12.

(56) Zivanov, J.; Nakane, T.; Forsberg, B.; Kimanius, D.; Hagen, W. J. H.; Lindahl, E.; Scheres, S. H. W. RELION-3: New Tools for Automated High-Resolution Cryo-EM Structure Determination. bioRxiv **2018**, 421123.

(57) Pettersen, E. F.; Goddard, T. D.; Huang, C. C.; Couch, G. S.; Greenblatt, D. M.; Meng, E. C.; Ferrin, T. E. UCSF Chimera—A Visualization System for Exploratory Research and Analysis. J. Comput. Chem. 2004, **25**, 1605–1612.

TABLE OF CONTENTS GRAPHIC